RSC Advances

PAPER

View Article Online
View Journal | View Issue

Effect of mesopore structure of TNU-9 on methane dehydroaromatization

Cite this: *RSC Adv.*, 2014, **4**, 26577

Jing Hu,[a] Shujie Wu,[a] Heng Liu,[a] Hong Ding,[b] Zhifang Li,[a] Jingqi Guan*[a] and Qiubin Kan*[a]

Received 30th April 2014
Accepted 27th May 2014

DOI: 10.1039/c4ra03945a

www.rsc.org/advances

A series of micro-mesoporous molecular sieves TNU-9-*x* (TNU-9 Taejon National University no. 9) were prepared by a hydrothermal reaction method for non-oxidative aromatization of methane. The physical properties of the synthesized samples were characterized by XRD, SEM, TEM, BET, NH_3-TPD and FT-IR spectroscopy. Characterization results suggested that the micro-mesoporous molecular sieves TNU-9-*x* exhibited similar geometrical shapes, but different pore properties with conventional microporous molecular sieve TNU-9. Catalytic tests indicated that Mo–TNU-9-20 showed excellent catalytic performance with a 14.9% conversion of methane and a 9.9% yield of aromatics. In addition, the catalytic stability of Mo–TNU-9-20 was better than the conventional microporous material Mo–TNU-9. The improved catalytic behaviour might be attributed to the generation of a secondary mesoporous system within the hierarchical pore materials.

1 Introduction

Due to abundant natural resources, the effective utilization of natural gas has attracted increasing attention during the past several decades. Methane dehydroaromatization (MDA) is considered as an efficient method for the direct conversion of methane into aromatics and hydrogen without oxygen participation. A non-oxidative aromatization catalyst Mo–ZSM-5 was reported by Wang *et al.* in 1993.[1] Mo–ZSM-5, having a unique 10-ring (10-membered ring) channel and a pore size close to benzene's kinetic diameter, has generally been regarded as one of the most appropriate catalysts for the methane dehydroaromatization reaction. However, due to the rapid deposition of polyaromatics and coke on the surface or in the channel of the catalyst with time-on-stream, it suffers a rapid decrease in methane conversion.[2] Many strategies, such as introducing various transition metal promoters,[3–5] introducing a second-component metal (*e.g.* Cu, Co, Ru, Fe, Pt, Ir, La, Ga or V),[6–9] introducing gas-phase additives (H_2, CO, CO_2, H_2O, *etc.*) to the reaction feed[10,11] and post-treatment or post-synthesis of catalyst support,[12–15] have been exploited to improve the catalytic activity and stability.

Moreover, it has been found that the status of molybdenum species (*i.e.* distribution of Mo species and formation of active Mo species) plays an essential role in methane aromatization. In addition, many researchers investigated the relationship between zeolite structures and catalytic properties. In the early work, researchers reported that HMCM-22 possesses a unique pore architecture with two independent pore systems with a 2D 10-ring sinusoidal pore system, and a larger 3D 12-ring supercage system inter-connected by 10-ring windows (4.0 × 5.5 Å). It was considered that the presence of supercages is responsible for the high coke accommodation ability of HMCM-22, while retaining shape selectivity of the 2D 10-ring sinusoidal pores is necessary for the formation of aromatics.[16,17] Moreover, a variety of zeolites with MWW-type topology structures (*e.g.* MCM-36,[18] MCM-49 (ref. 19)) were also tested in the non-oxidative aromatization of methane and found to exhibit high catalytic activity, but low selectivity to benzene and low catalytic stability. In addition, ITQ-2, which has been prepared by delamination of the layered precursor of MCM-22, has been also applied in the non-oxidative aromatization of methane.[20] The acid-treated ITQ-2 performed more selectively compared to benzene for the Mo/MCM-22 catalyst. Recently, our group found that Mo–TNU-9 exhibited excellent catalytic performance in non-oxidative aromatization of methane.[21] TNU-9 possesses a 3D 10-ring channel system ([010] 5.6 × 5.5 Å, [101] 5.4 × 5.5 Å), as well as large 3D 12-ring cavities (around 7.2 Å) that are accessible only through 10-ring windows.

With regard to the catalytic behavior of zeolite, acidity assessment is also of critical importance. It is well known that concentration, location and acid strength of Brønsted and Lewis acid sites have great influence on the rate of reactions.[22,23] FTIR spectroscopy is usually used to determine the type, strength and concentration of acid sites of zeolites using different basic probe molecules, and the results can be related

[a]*College of Chemistry, Jilin University, Changchun, 130023, PR China. E-mail: guanjq@jlu.edu.cn; qkan@mail.jlu.edu.cn*

[b]*State Key Laboratory of Inorganic Synthesis and Preparative Chemistry, College of Chemistry, Jilin University, Changchun 130012, P.R. China*

to theoretical calculations. Furthermore, NH_3-TPD is also crucial for the determination of zeolite acidity.[24]

Extending the application of hierarchical zeolites has long been a driving force for improving the catalytic activity of MDA. The creation of a proper mesoporosity in the zeolite system has been successfully accomplished. Through the post-treatment of synthesized zeolites or the templating method during the zeolite crystallization, such as colloid-imprinted carbons,[25] cationic polymers,[26,27] amphiphilic organosilane surfactant,[28] and silane-functionalized polymer,[29] an additional mesoporous system can be introduced. In this paper, we attempted to prepare TNU-9 with a mesoporous structure for methane dehydroaromatization.

2 Experimental

2.1. Catalyst preparation

TNU-9 zeolite was synthesized by a hydrothermal process with 1,4-bis(methylpyrrolidinium) pentane (1,4-MPP) as a template and phenyltriethoxysilane (PTEOS) as the mesoporous maker. In a typical synthesis, a certain amount of 1,4-MPP was added into a vessel with water. Then, aluminum nitrate nonahydrate, sodium hydroxide, phenyltriethoxysilane and fumed silica were successively introduced into the vessel with vigorous stirring for 24 h. The final synthesized gels had the following chemical composition: 100-$x$$SiO_2$: 36.67$Na_2O$: xPTEOS: 2Al_2O_3: 15(1,4-MPP): 4000H_2O (x = 0, 15, 20, 25). The gels were crystallized in Teflon-lined autoclaves at 170 °C with constant stirring at 60 rpm for 10 days. After crystallization, the solid was washed, dried and finally calcined at 550 °C for 5 h to obtain Na/TNU-9-x (x represents the content of PTEOS). H/TNU-9-x was prepared by repeating the ion exchange of the calcined Na/TNU-9-x three times with a 1 mol L^{-1} of ammonium nitrate solution at 90 °C, followed by calcination in air at 500 °C for 4 h. Molybdenum oxide (MoO_3, Beijing Chemical Works, 99.5% purity) was physically mixed by grinding with H/TNU-9-x to prepare the sample containing 6 wt% of MoO_3, and then the catalyst was calcined in air at 500 °C for 3 h to obtain Mo–TNU-9-x.

2.2. Catalyst characterization

XRD measurements were performed by using CuKα radiation on the Shimadzu XRD-6000 diffractometer. The SEM photographs were obtained on a FESEM XL-30 field-emission scanning electron microscope. The TEM images were obtained with a HITACHI H-8100 electron microscope, which is operated at an accelerating voltage of 200 kV. The BET surface area was obtained through the BET (Brunauer–Emmett–Teller) method, and the average pore volume was measured with t-plot analysis. N_2 adsorption–desorption isotherms were performed with a Micromeritics ASAP 2020 system at −196 °C. The sample was outgassed at 250 °C for 3 h before measurement. IR spectra were recorded by a Fourier transform infrared (FTIR) spectrometer, in which samples (30 mg) were pressed in self-supporting discs (diameter 1.2 cm) and pretreated under vacuum at 450 °C for 6 h. Pyridine was adsorbed on the samples at 100 °C, and the samples were followed by an outgas process *in situ* under vacuum at 100 °C for 1 h in order to remove physically adsorbed molecules. The density of the Brønsted and Lewis acid sites was calculated from the integrated areas of the bands at 1548 cm^{-1} and 1448 cm^{-1}, respectively, according to the method reported by Gil *et al.*[30] NH_3-TPD was performed on a conventional setup equipped with a thermal conductivity detector (TCD).

2.3. Catalytic tests

The catalytic tests were performed under atmospheric pressure through a continuous-flow fixed-bed quartz reactor of 1 cm ID with 0.5 g of 40–60 mesh-sized catalyst. The feed mixture gas of 92.5% CH_4 and 7.5% N_2 at 1500 mL g^{-1} h^{-1} was introduced through a mass flow controller, and the temperature was raised to 700 °C within 45 min. An online gas chromatograph (GC-17A) was equipped with a 6 m × 3 mm HayeSep D 80/100 column and a TCD detector to analyze H_2, N_2, CO, CO_2, CH_4, C_2H_4, and C_2H_6, as well as a CBP1-M50-025 (Shimadzu) quartz capillary column and an FID detector to analyze benzene, toluene and naphthalene. Helium was used as the carrier gas and an N_2 internal standard analyzing method similar to that reported by Ichikawa *et al.*[4] was used to calculate the conversion of methane and selectivity to hydrocarbon products according to the carbon mass balance.

3 Results and discussion

3.1. XRD studies

The wide-angle XRD patterns of all TNU-9-x catalysts are shown in Fig. 1. TNU-9-0 shows well-resolved peaks that are characteristic reflections for typical crystalline TNU-9 structure, which is in accordance with the literature.[21] After the introduction of organosilane, the samples basically preserved the lattice structure of the TNU-9 zeolite.

3.2. SEM and TEM studies

The SEM images of the conventional TNU-9 (denoted as TNU-9-0 here) and TNU-9-20 are shown in Fig. 2. TNU-9-0 contains coffin-shape crystals with high crystallinity, which is in accordance with the literature.[31] In addition, TNU-9-20 (Fig. 2b) also

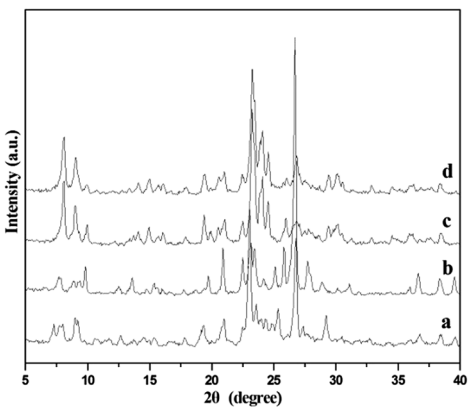

Fig. 1 XRD patterns of (a) TNU-9-0, (b) TNU-9-15, (c) TNU-9-20 and (d) TNU-9-25.

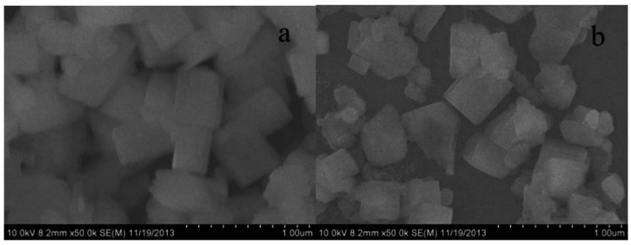

Fig. 2 SEM images of samples: (a) TNU-9-0 and (b) TNU-9-20.

shows the presence of cubical-shaped crystals, but the distribution of particle size is wide in the range of 0.1–0.5 μm.

The TEM images of TNU-9-0 and TNU-9-20 are shown in Fig. 3. It can be seen that both samples are synthesized in coffin-shaped crystals. In addition, TNU-9-20 presents a mixture of zeolitic phases (marked with a rectangle) and some mesoporous phases (marked with a circle), as shown in Fig. 3d, whereas mesopore phases could not be observed in the conventional TNU-9-0 (Fig. 3a and b).[32] The TEM images prove that the PTEOS might successfully create secondary mesoporous systems within zeolite crystals.

3.3. N_2 adsorption–desorption studies

Nitrogen adsorption–desorption isotherms of TNU-9-*x* are shown in Fig. 4. The TNU-9-0 shows the type I isotherm with a high nitrogen uptake at low relative pressures, which is characteristic for purely microporous materials. The isotherm of the PTEOS-treated TNU-9-*x* is a combination of a type I and type IV isotherm, typical for hierarchical materials. The uptake of

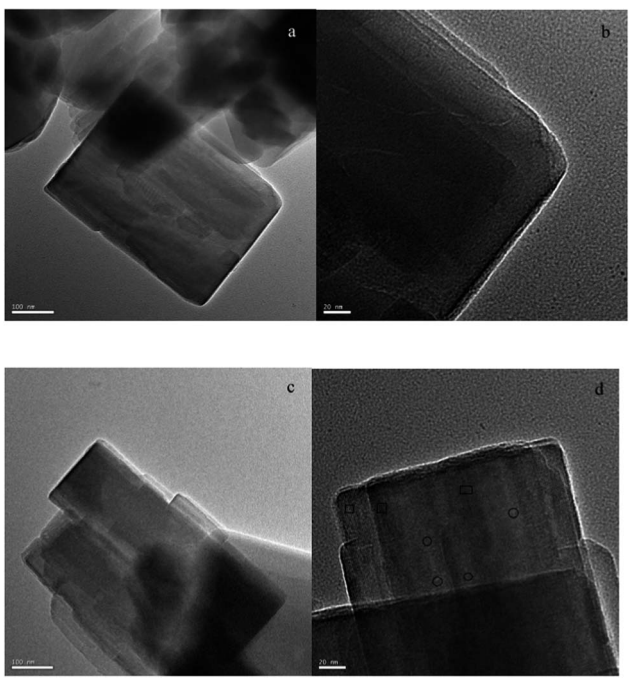

Fig. 3 TEM images of samples: (a and b) TNU-9-0 and (c and d) TNU-9-20.

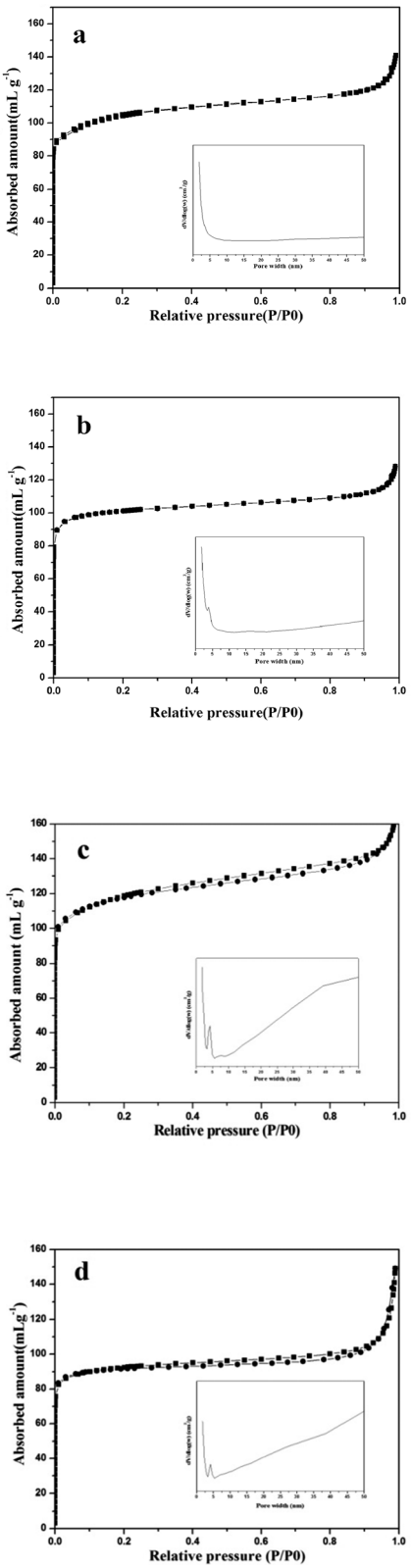

Fig. 4 Nitrogen adsorption and desorption isotherms of (a) TNU-9-0, (b) TNU-9-15, (c) TNU-9-20 and (d) TNU-9-25.

nitrogen could be increased significantly in the low relative pressure region, as well as at pressures above $p/p^0 = 0.3$. The distinctive increase in adsorption capacity at $p/p^0 = 0.4$–0.9

Table 1 The textural properties of TNU-9-0, TNU-9-15, TNU-9-20 and TNU-9-25

Samples	S_{BET}	$S_{micropore}$ ($m^2\ g^{-1}$)	$V_{micropore}$ ($cm^3\ g^{-1}$)	$V_{mesopore}$ ($cm^3\ g^{-1}$)	V_{toltal} ($cm^3\ g^{-1}$)
TNU-9-0	359	286	0.13	0.06	0.19
TNU-9-15	374	267	0.12	0.08	0.20
TNU-9-20	386	266	0.12	0.11	0.23
TNU-9-25	362	257	0.12	0.10	0.22

reveals that the presence of mesopores in a size range from 3 to 10 nm, whereas TNU-9-0 sample does not display such kind of hysteresis loop, which suggests that a certain amount of mesopores have been formed in TNU-9-15, TNU-9-20 and TNU-9-25. Correspondingly, the pore-size distribution of the calcined TNU-9-15, TNU-9-20 and TNU-9-25 calculated from the desorption branch of the isotherm shows a narrow peak centered at 4.2 nm. Moreover, the specific BET surface area, the total pore volume, the micropore volume and the mesopore volume are briefly summarized in Table 1. The mesoporous volume slightly increases, accompanied with increase in the concentration of PTEOS, which would reach a maximum when the concentration of PTEOS increases up to 20%, and then decrease with further increase in the concentration of PTEOS. The change of the mesopore-specific surface area of TNU-9-*x* shows a similar trend with the change of mesoporous volume. The micropore volume and the micropore-specific surface area decrease with increase in PTEOS in the synthesized system. This might demonstrate that only a portion of PTEOS could participate in the mesopore construction of TNU-9, whereas an over-abundance of PTEOS may result in the collapse of partial mesoporous structures during the calcination process, which leads to the reduction in the mesoporous volume.

3.4. Acidity tests

The results of NH_3-TPD for H-TNU-9-*x* and 6Mo–TNU-9-*x* are shown in Fig. 5. H-TNU-9-*x* shows two peaks, which is similar to H-ZSM-5.[33] The two peaks are denoted as peak H and peak L, and they are centered at about 412 °C and 213 °C, respectively. For NH_3-TPD profiles of the Mo–TNU-9-*x* zeolite, there were three peaks after curve fitting of the NH_3-TPD peaks, which are located at *ca.* 213, 310 and 412 °C, respectively. The peak at 213 °C is attributed to the desorption of the physisorbed NH_3 species and/or NH_3 adspecies residing on non-exchangeable cationic sites, whereas the peak at 310 °C is assigned to the desorption of NH_3 adspecies adsorbed on exchangeable protonic sites. Finally, the peak at 412 °C is attributed to strong Lewis acid sites. It is understandable that the difference in the peak temperatures may be mainly resulted from the samples with different SiO_2/Al_2O_3 ratios.

For the HTNU-9-*x* catalysts, the quantitative acidic results have been listed in Table 2. It shows that the areas of both peaks L and H decrease with the introduction of PTEOS, which can demonstrate that the introduction of PTEOS influences the SiO_2/Al_2O_3 ratios for HTNU-9-*x*. Moreover, a new peak emerges

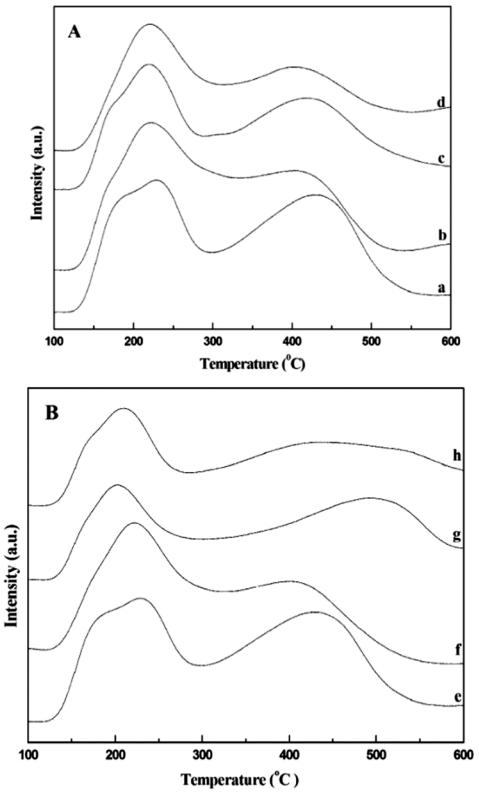

Fig. 5 NH_3-TPD profiles of the catalysts: (a) H-TNU-9-0, (b) Mo–TNU-9-0, (c) H-TNU-9-15, (d) Mo–TNU-9-15, (e) H-TNU-9-20, (f) Mo–TNU-9-20, (g) H-TNU-9-25 and (h) Mo–TNU-9-25.

at *ca.* 310 °C after loading 6% MoO_3, which is denoted as peak M. This indicates that the Mo species should interact with the Brønsted acid sites and generate the medium-strength acid sites. On the other hand, it can be found the high-temperature peak obviously decreased with increase in the concentration of molybdenum due to the lowering of the amount of Brønsted sites, which results from modification/interaction of Mo ions. Furthermore, the Brønsted acid sites decrease approximately by *ca.* 45% after loading 6% MoO_3 for all of zeoilite TNU-9-*x*, indicating that the Mo species should migrate into the channels and locate themselves close to the Brønsted acid sites of the TNU-9 zeolite.

The acidities of H-TNU-9-*x* and Mo-containing Mo–TNU-9-*x* have further been studied by FTIR-pyridine after desorption of pyridine at 100 °C (Fig. 6). It is apparent from the figure that the absorption peaks emerging at *ca.* 1548 and 1448 cm^{-1} can be assigned to the Brønsted and Lewis acid sites, respectively.[34] We have made a quantitative calculation, and the data are listed in Table 3. From Fig. 6 and Table 3, both the Brønsted and Lewis acid relative amounts decrease with increasing PTEOS concentration among the four TNU-9-*x* samples. Thus, it can be concluded that mesopores would affect the zeolitic acidity. In addition, it can be confirmed from Fig. 6 that the total acid amount of the Brønsted and Lewis acids for Mo–TNU-9-*x* decreases in comparison with the corresponding H-TNU-9-*x*, particularly for the Brønsted acid, which can afford further

Table 2 Peak temperatures of NH_3-TPD spectra and the corresponding amounts of acid sites of H/TNU-9-*x* and Mo–TNU-9-*x*

	Peak (L)		Peak (M)		Peak (H)		
Samples	Peak temp (°C)	Area arb. unit	Peak temp (°C)	Area arb. unit	Peak temp (°C)	Area arb. unit	Total
TNU-9-0-H	213	420	—	—	417	528	948
TNU-9-0–Mo	211	362	309	243	408	267	872
TNU-9-15-H	208	295	—	—	415	381	676
TNU-9-15–Mo	214	212	307	194	410	214	620
TNU-9-20-H	207	268	—	—	418	354	622
TNU-9-20–Mo	212	206	307	157	412	198	561
TNU-9-25-H	205	238	—	—	410	275	513
TNU-9-25–Mo	204	197	306	124	398	154	475

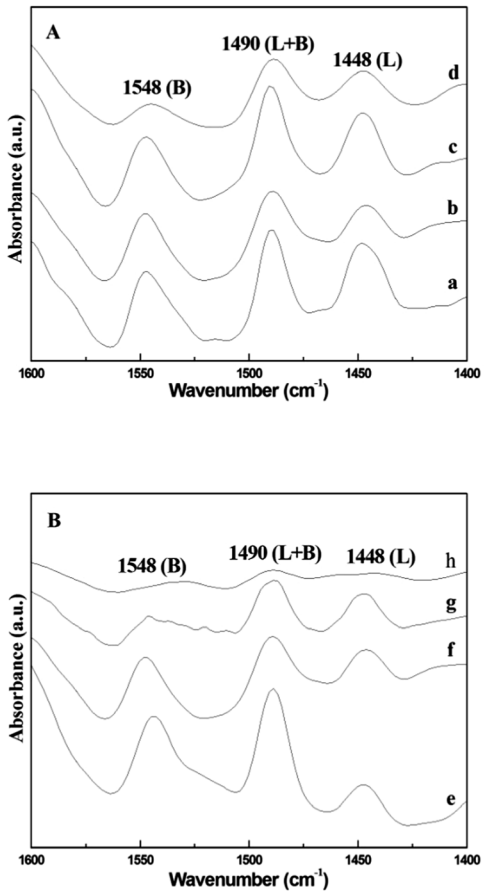

Fig. 6 FTIR spectra in the pyridine region after desorption of the base at 100 °C for the zeolites and Mo-loaded catalysts: (a) H-TNU-9-0, (b) Mo–TNU-9-0, (c) H-TNU-9-15, (d) Mo–TNU-9-15, (e) H-TNU-9-20, (f) Mo–TNU-9-20, (g) H-TNU-9-25 and (h) Mo–TNU-9-25.

proof that the Mo species may interact with the Brønsted acid sites in agreement with the abovementioned NH_3-TPD results. The results suggest that Mo species should migrate into the channels of the zeolite and interact with the Brønsted acid Al–OH to form Al–O–Mo species.[24]

3.5. Catalytic test

A series of Mo–TNU-9-*x* zeolites were investigated for the non-oxidative aromatization of methane at 700 °C. It was reported that the 6 wt% of Mo content supported on TNU-9 was optimized for this reaction in our previous work.[21] Therefore, in this study, 6 wt% of Mo content was supported on various H/TNU-9-*x* catalysts. The catalytic results are listed in Table 4, and the effect of time on the stream on the catalytic behavior of methane aromatization is depicted in Fig. 7. From Table 4, it can be found that the catalytic performance of Mo–TNU-9-15 is slightly better than that of Mo–TNU-9-0, whereas it is exciting to note that Mo–TNU-9-20 shows 9.9% yield of aromatics, which is far higher than Mo–TNU-9-0. However, with further increase in the content of PTEOS, the catalytic behavior of Mo–TNU-9-25 is lesser than Mo–TNU-9-0. The catalytic result is similar to our previous report on PTEOS-modified ZSM-5.[35]

From Fig. 7, the methane conversion over the four catalysts rises sharply in the beginning of the reaction, and reaches a maximum after reaction for 80 min, which is attributed to the existence of the induction period. The highest methane conversion over Mo–TNU-9-0, Mo–TNU-9-15, Mo–TNU-9-20 and Mo–TNU-9-25 is 11.3%, 11.4%, 14.9% and 8.9%, respectively. After that, the conversion of methane decreases with time-on-stream and remains relatively stable after reaction for 300 min. Moreover, at this time, the methane conversion over Mo–TNU-9-0, Mo–TNU-9-15, Mo–TNU-9-20 and Mo–TNU-9-25 is 6.3%, 8.4%, 10.3% and 5.7%, respectively. It is supposed that the Mo species (MoC_x or MoO_xC_y) are the active center during the process of methane activation (induction period), whereas acid sites, particularly for the appropriate Brønsted acid sites that distribute within the channels of zeolites, are beneficial for the formation of benzene and other aromatics in the MDA reaction.[36]

The yields of benzene and naphthalene over the four catalysts are shown in Fig. 7, and the selectivities to benzene, toluene, naphthalene and coke are listed in Table 4. Mo/TNU-9-20 shows the highest yield for benzene and naphthalene among the four catalysts. Moreover, the yield of benzene is in the following order: Mo–TNU-9-20 > Mo–TNU-9-15 ≈ Mo–TNU-9-0> Mo–TNU-9-25, whereas the yield of naphthalene is as follows: Mo–TNU-9-20 > Mo–TNU-9-15 > Mo–TNU-9-25 ≈ Mo–TNU-9-0. From Table 4, it can be found that the selectivity to benzene over PTEOS-modified catalysts (Mo–TNU-9-15, Mo–TNU-9-20 and Mo–TNU-9-25) is lower than that over Mo–TNU-9-0, whereas the selectivity to naphthalene shows an opposite trend. For

Table 3 Quantitative results from pyridine-FTIR of HTNU-9-*x*

	Catalysts			
Concentration	TNU-9-0	TNU-9-15	TNU-9-20	TNU-9-25
Bronsted acid sites (mmol g^{-1})	0.2435	0.2347	0.2258	0.2078
Lewis acid sites (mmol g^{-1})	0.1136	0.1031	0.0881	0.0443
Total acid sites (mmol g^{-1})	0.3571	0.3378	0.3139	0.2521

Table 4 Catalytic results of the aromatization of methane over Mo–TNU-9-*x* and H-TNU-9-20 at 80 min[a]

		Selectivity (%)				
Catalyst	Conversion of CH_4 (%)	Benzene	Toluene	Naphthalene	Coke	Yields of aromatics (%)
Mo–TNU-9-0	11.3	42.7	2.3	9.0	46.0	6.1
Mo–TNU-9-15	11.4	42.4	1.8	11.7	44.1	6.4
Mo–TNU-9-20	14.9	38.9	1.7	25.9	33.5	9.9
H-TNU-9-20	Trace	—	—	—	—	—
Mo–TNU-9-25	8.9	39.2	1.3	14.6	44.9	4.9

[a] Reaction condition: $T = 973$ K, 1 atm, GHSV = 1500 h^{-1}.

example, the selectivity to naphthalene can reach up to 25.9% over Mo–TNU-9-20 after an 80 min reaction time, whereas the selectivity to naphthalene is 9.0% over the conventional Mo–TNU-9-0.

It has been reported that the channel structure, crystal size, acidity of the catalyst, the location of the Mo species and the nature of the active Mo species might affect the catalytic performance of the catalyst in methane non-oxidative aromatization. According to the abovementioned characterization results, the introduction of PTEOS would lead the production of mesoporous structures in the synthesized materials, which might be one of the key factors for the better catalytic performance of Mo–TNU-9-20.[35,37] However, modification with excess organosilane (*i.e.* 25% content of PTEOS) may result in the partial collapse of the catalyst's structure during the calcination process, thus decreasing the catalytic performance. Many researchers have conducted a considerable amount of study on the catalytic behavior of Mo–ZSM-5 in non-oxidative aromatization of methane and found that hierarchical ZSM-5 showed better catalytic performance than conventional ZSM-5. Martínez *et al.* prepared mesopore-containing ZSM-5 by carbon template and found that the mesoporous structure can effectively enhance the stability of Mo–ZSM-5 in methane aromatization.[24] For example, the yield of aromatics could reach 3% over Mo–ZSM-5 with mesoporous structures, whereas the yield of aromatics decreased down to *ca.* 2% over conventional Mo–ZSM-5 after a reaction for 8 h. Moreover, it was reported that the hierarchical structure is beneficial for the dispersal of the active species and results in well-dispersed active species throughout the zeolite.[38,39] The results of nitrogen adsorption and desorption isotherms (Fig. 4 and Table 1) clearly show that PTEOS modified catalysts Mo–TNU-9-15, Mo–TNU-9-20 and Mo–TNU-9-25 have a certain amount of mesoporous structure, particularly for Mo–TNU-9-20, in which the mesoporous volume is the largest. Moreover, there is general consensus that a 10-ring 2D channel and Brønsted sites play key roles in the methane conversion. The 3D channel system with cavity structure allows TNU-9 to better generate, accommodate and diffuse of aromatics in the reaction. In this case, hierarchical TNU-9-20 makes Mo species more rapidly transfer into the channels and make them associate with Brønsted acid sites. It has been reported that Brønsted acid sites might give rise to the deposition of aromatic-type coke, and the excessive amount of Brønsted acid sites would lead to catalyst deactivation. As shown by the results of NH_3-TPD and IR spectra of pyridine adsorption, Mo species can react with Brønsted acid sites and properly adjust the acid amount of the materials.

It is widely accepted that benzene is mainly formed in the channel of the zeolite catalyst, whereas naphthalene is produced on the external surface, the pore mouth of the channel or in the mesoporous channel of the zeolite due to the larger dynamic diameter of naphthalene compared to the micropore channel. Therefore, it is no wonder that the selectivity to naphthalene over PTEOS-modified Mo–TNU-9-*x* is generally higher than that of Mo–TNU-9-0. In addition, from Table 4, the yield of carbonaceous deposition for TNU-9-20 is lower than conventional TNU-9-0. Accordingly, it is suggested that the hierarchical structure of TNU-9-20 prompts the dispersion of MoO_x into the TNU-9-20 channel and makes the MoO_x species accessible to Brønsted acid sites, thus remarkably enhancing methane conversion and benzene yield.

Considering the fabrication of polyaromatics and coke, it has been suggested that mass transformation is an important influencing factor. TG profiles of the coked Mo–TNU-9-0 and Mo–TNU-9-20 catalysts are shown in Fig. 8. As is well known, the weight loss at 100–220 °C is mainly due to evaporation of

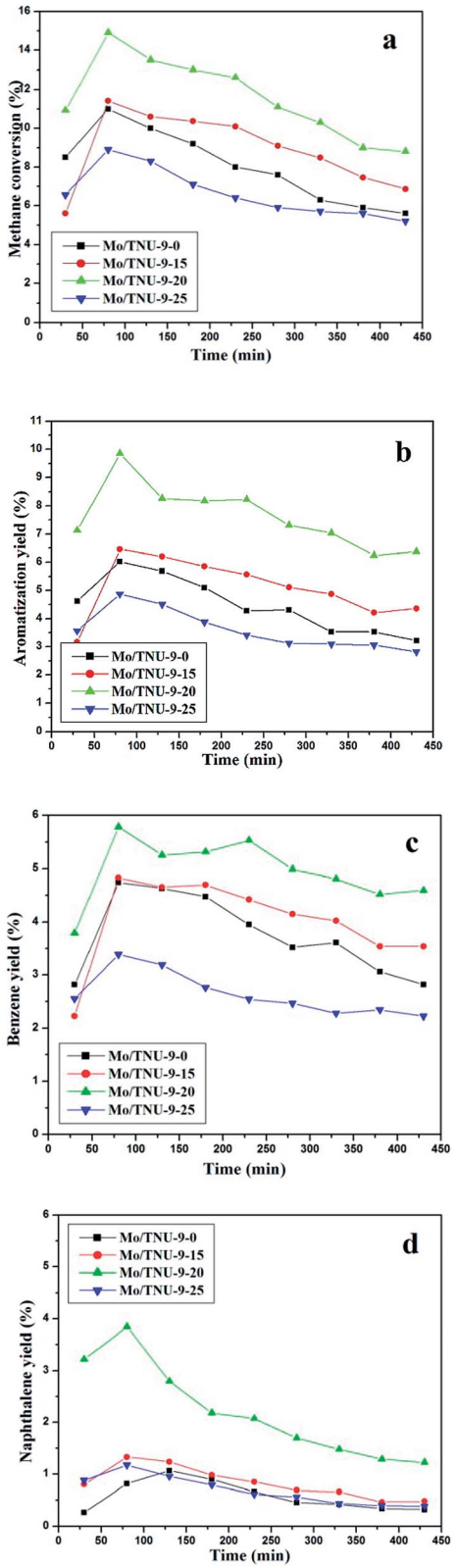

Fig. 7 The comparison of catalytic performance for methane aromatization over Mo–TNU-9-0 (■), Mo–TNU-9-15(●), Mo–TNU-9-20 (▲), and Mo–TNU-9-25 (▼). Reaction condition: $T = 700$ °C, $P =$ 1 atm, GHSV = 1500 h^{-1}.

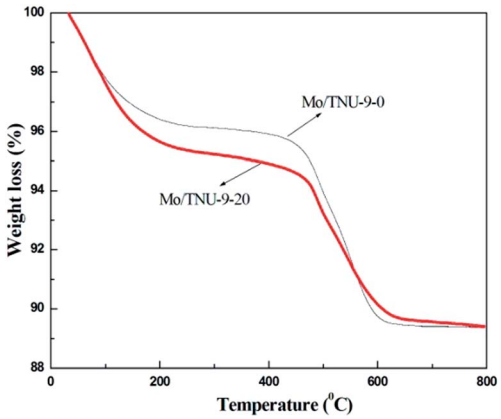

Fig. 8 TG analysis of Mo–TNU-9-0 and Mo–TNU-9-20.

physisorbed and chemisorbed water, whereas the weight loss under 400 °C could be attributed to the physical absorption of aromatics. However, weight loss in the range of 400 –800 °C was attributed to the decomposition of coke. The coked Mo–TNU-9-20 catalyst after 300 min of reaction time exhibits a weight loss of *ca.* 6.0%, whereas the coked Mo–TNU-9-0 catalyst after 300 min of reaction time shows about 7.1% weight loss. The selectivity to the coke for Mo–TNU-9-20 was also lower than that for Mo–TNU-9-0 (see Table 4). Therefore, the average rate of coke formation on the Mo–TNU-9-20 catalyst is lower than that on the Mo–TNU-9-0 catalyst. It is well known that the deposition of polyaromatics and coke is the main reason for the deactivation of the catalyst.[36,39] The carbonaceous deposits may cover the Brønsted acid sites, and therefore gradually lead to the loss of partial active sites and the blockage of the zeolite channels, thus making some efficient active sites inaccessible for the reactant and reaction intermediates. Therefore, it can be concluded that the different degree of deactivation over two zeolites may be ascribed to the different content of carbonaceous deposits formed on/in the catalysts during the reaction.

4 Conclusions

A series of TNU-9-*x* with micro-mesoporous structures have been successfully prepared by introducing different contents of PTEOS into the synthesis system, and the resultant materials were applied for the aromatization of methane. BET and TEM demonstrated that the introduction of PTEOS led to the production of mesopore. NH_3-TPD and FT-IR showed that Mo species interacted with the Brønsted acid and decreased the acidic amount of the materials. Mo–TNU-9-20 showed higher methane conversion and higher yields of benzene and naphthalene than Mo–TNU-9-0, Mo–TNU-9-15, and Mo–TNU-9-25 under the same experimental conditions. Furthermore, micro-mesoporous Mo–TNU-9-20 exhibited better catalytic stability than pure microporous Mo–TNU-9-0 in the methane aromatization reaction.

Acknowledgements

This work was supported by the National Natural Science Foundation of China (21303069) and Jilin province (201105006).

Notes and references

1 L. Wang, L. Tao, M. Xie, G. Xu, J. Huang and Y. Xu, *Catal. Lett.*, 1993, **21**, 35–41.
2 L. Chen, L. Lin, Z. Xu, T. Zhang and X. Li, *Catal. Lett.*, 1996, **39**, 169–172.
3 Y. Xu and L. Lin, *Appl. Catal., A*, 1999, **188**, 53–67.
4 S. Liu, Q. Dong, R. Ohnishi and M. Ichikawa, *Chem. Commun.*, 1997, 1455–1456.
5 R. Kojima, S. Kikuchi, H. Ma, J. Bai and M. Ichikawa, *Catal. Lett.*, 2006, **110**, 15–21.
6 M. C. Iliuta, B. P. Grandjean and F. Larachi, *Ind. Eng. Chem. Res.*, 2003, **42**, 323–330.
7 S. Li, C. Zhang, Q. Kan, D. Wang, T. Wu and L. Lin, *Appl. Catal., A*, 1999, **187**, 199–206.
8 T. Pinglian, X. Zhusheng, Z. Tao, C. Liayuan and L. Liwu, *React. Kinet. Catal. Lett.*, 1997, **61**, 391–396.
9 B. Liu, Y. Zhang, J. Liu, M. Tian, F. Zhang, C. Au and A.-C. Cheung, *J. Phys. Chem.*, 2011, **115**, 16954–16962.
10 R. Ohnishi, S. Liu, Q. Dong, L. Wang and M. Ichikawa, *J. Catal.*, 1999, **182**, 92–103.
11 A. C. C. Rodrigues and J. L. F. Monteiro, *Catal. Commun.*, 2008, **9**, 1060–1065.
12 W. Ding, G. D. Meitzner and E. Iglesia, *J. Catal.*, 2002, **206**, 14–22.
13 Y. Lu, D. Ma, Z. Xu, Z. Tian, X. Bao and L. Lin, *Chem. Commun.*, 2001, 2048–2049.
14 A. C. C. Rodrigues and J. L. F. Monteiro, *Catal. Lett.*, 2007, **117**, 166–170.
15 L. Su, L. Liu, J. Zhuang, H. Wang, Y. Li, W. Shen, Y. Xu and X. Bao, *Catal. Lett.*, 2003, **91**, 155–167.
16 Y. Wu, X. Ren, Y. Lu and J. Wang, *Mater. Lett.*, 2008, **62**, 317–319.
17 X. Yin, N. Chu, J. Yang, J. Wang and Z. Li, *Catal. Commun.*, 2013, **43**, 218–222.
18 P. Wu, Q. Kan, D. Wang, H. Xing, M. Jia and T. Wu, *Catal. Commun.*, 2005, **6**, 449–454.
19 P. Yang, J. Yu, N. Xu, J. Wang and T. Wu, *Catal. Commun.*, 2007, **8**, 997–1002.
20 A. Martínez, E. Peris and G. Sastre, *Catal. Today*, 2005, **107**, 676–684.
21 H. Liu, S. Yang, S. Wu, F. Shang, X. Yu, C. Xu, J. Guan and Q. Kan, *Energy*, 2011, **36**, 1582–1589.
22 Z. Musilová, N. Žilková, S.-E. Park and J. Čejka, *Top. Catal.*, 2010, **53**, 1457–1469.
23 M. Kubů, N. Žilková and J. Čejka, *Catal. Today*, 2011, **168**, 63–70.
24 A. Martínez, E. Peris, M. Derewinski and A. Burkat-Dulak, *Catal. Today*, 2011, **169**, 75–84.
25 S.-S. Kim, J. Shah and T. J. Pinnavaia, *Chem. Mater.*, 2003, **15**, 1664–1668.
26 Q. Huo, Y. Gong, T. Dou, Z. Zhao, H. Pan and F. Deng, *Energy Fuels*, 2010, **24**, 3764–3771.
27 X. Meng, F. Nawaz and F.-S. Xiao, *Nano Today*, 2009, **4**, 292–301.
28 M. Choi, H. S. Cho, R. Srivastava, C. Venkatesan, D.-H. Choi and R. Ryoo, *Nat. Mater.*, 2006, **5**, 718–723.
29 K. Cho, H. S. Cho, L.-C. De Menorval and R. Ryoo, *Chem. Mater.*, 2009, **21**, 5664–5673.
30 B. Gil, S. I. Zones, S.-J. Hwang, M. Bejblová and J. Cejka, *J. Phys. Chem.*, 2008, **112**, 2997–3007.
31 M. T. Portilla, F. J. Llopis, C. Martínez, S. Valencia and A. Corma, *Appl. Catal., A*, 2011, **393**, 257–268.
32 F. N. Gu, F. Wei, J. Y. Yang, N. Lin, W. G. Lin, Y. Wang and J. H. Zhu, *Chem. Mater.*, 2010, **22**, 2442–2450.
33 Y. Shu, Y. Xu, S.-T. Wong, L. Wang and X. Guo, *J. Catal.*, 1997, **170**, 11–19.
34 J. M. Arandes, I. Torre, M. J. Azkoiti, J. Erena, M. Olazar and J. Bilbao, *Energy Fuels*, 2009, **23**, 4215–4223.
35 C. Xu, H. Liu, M. Jia, J. Guan, S. Wu, T. Wu and Q. Kan, *Appl. Surf. Sci.*, 2011, **257**, 2448–2454.
36 N. Chu, J. Yang, J. Wang, S. Yu, J. Lu, Y. Zhang and D. Yin, *Catal. Commun.*, 2010, **11**, 513–517.
37 H. Liu, S. Yang, J. Hu, F. Shang, Z. Li, C. Xu, J. Guan and Q. Kan, *Fuel Process. Technol.*, 2012, **96**, 195–202.
38 K. Egeblad, C. H. Christensen, M. Kustova and C. H. Christensen, *Chem. Mater.*, 2007, **20**, 946–960.
39 W.-C. Li, A.-H. Lu, R. Palkovits, W. Schmidt, B. Spliethoff and F. Schüth, *J. Am. Chem. Soc.*, 2005, **127**, 12595–12600.